

# Well-designed sandwich-like structured graphene/emeraldine salts prepared by inverse microemulsion polymerization with particle-on-sheet and sheet-on-sheet morphologies

Zahra Kachoei · Sepideh Khoee · Naser Sharifi Sanjani

Received: 29 August 2014 / Accepted: 2 February 2015 / Published online: 24 February 2015  
© Iran Polymer and Petrochemical Institute 2015

**Abstract** In this work, nanocomposites with well-designed sheet-on-sheet and particle-on-sheet structures consisting of emeraldine salt and graphene were prepared via in situ inverse microemulsion of aniline monomers by well-dispersed graphene as efficient template. Influences of the weight percentage of graphene on the morphology and electrical conductivity property of the resulting sandwich-like structures were discussed. All the materials were characterized by XRD, FTIR, DSC, Raman and UV–Vis spectroscopy techniques. The formation of emeraldine salt (ES) shell layer on the exterior of graphene was investigated by scanning electron microscopy (SEM) and transmission electron microscopy (TEM) techniques. The thermal stability, electrical conductivity and electrochemical property of the graphene/emeraldine salt nanocomposites were examined by thermogravimetric analysis (TGA), conventional four-probe method and cyclic voltammetry, respectively. In comparison with the pure emeraldine salt, the graphene/emeraldine salt sandwich-like structures showed enhanced electric conductivity, thermal stability and electrochemical property. A high specific capacitance of 1,615.42 F/g was obtained for graphene/emeraldine salt nanocomposites with sheet-on-sheet morphology at scan rate 5 mV/s which is superior to any studied graphene/emeraldine salt composites, up to now. Improvement in these properties is arisen from the fact that the  $\pi$ -bonded surface of the graphene sheet interacts strongly with the conjugated structure of the emeraldine salt sheet and increases relative amounts of quinoid rings to benzoid rings in sandwich-like structure of graphene/emeraldine salt nanocomposite.

**Keywords** Emeraldine salt · Graphene · Sandwich-like structure · Conducting polymer · Inverse microemulsion

## Introduction

The combination of carbonaceous nanostructures (such as graphene) and conjugated polymers (e.g., emeraldine salt) enhances the possibility of exploring novel materials offering well-designed mechanical, electrical, optical, thermoelectric and electrochromic properties [1]. Graphene/emeraldine salt nanocomposites have great potentials in applications such as rechargeable batteries, supercapacitors, electromagnetic interference (EMI) shielding and sensors [2–4].

Since 2004, that graphene, as a single layer of carbon atoms, was discovered by Geim [5], and it has attracted a great deal of attention, due to its extraordinary electric, thermal and mechanical properties [6] and potentially low manufacturing cost [7]. Moreover, graphene nanosheets exhibit large surface-to-volume ratio [8] which renders them as attractive substrate materials when compounded with polymers and inorganic particles for lithium ion batteries [9, 10], electrochemical capacitors [11] or optical transparent films [12].

One means of developing the electrochemical properties of graphene-based composite materials is the possibility of thinning the graphene sheets and properly dispersing them in the composite matrix. Therefore, the uniform dispersion of graphene nanosheets in the polymer matrix is one of the critical factors in enhancing the physical properties of nanocomposites [13]. There have been many attempts to uniformly incorporate graphene sheets into composite materials. For example, a good dispersion of functionalized graphene sheets in polymer matrix was achieved, and

Z. Kachoei · S. Khoee (✉) · N. Sharifi Sanjani  
Polymer Laboratory, Chemistry Department, School of Science,  
University of Tehran, P.O. Box: 14155-6455, Tehran, Iran  
e-mail: Khoee@khayam.ut.ac.ir

polymer-based composites showed better mechanical and highly increased thermal properties at especially low loading of the graphene [14]. However, because of functionalization of graphene sheets, their electrical conductivity was reduced. Among numerous conductive polymers, emeraldine salt (ES) is one of the best conjugated conducting polymers because of its promising electron transport properties. Emeraldine salt shows promising polymer applications because of its unique properties, simple synthesis, low cost, controllable electrical conductivity and interesting redox properties that are associated with its nitrogen atoms [15]. Moreover, emeraldine salt has the highest environmental stability and is recognized as the only conducting polymer stable in air [16]. Emeraldine salt composites prepared with various materials have received great attention because of their superior processability, moderately good mechanical properties, good conductivity and unique applications in various electrical and chemical devices. The excellent properties of graphene and the advantages of emeraldine salt have fascinated great research concerns in preparing graphene/ES composites.

Many studies have been done to synthesize PANI/graphene composites in order to combine the high stability, high surface area and conductivity of graphene with PANI. Both in situ polymerization and solution blending methods have been used to prepare the composite in literatures. Many researchers produced PANI/graphene composites via mixing of graphene sheets and PANI nanowires. Liu et al. [17] made graphene/polyaniline film sheets by vacuum filtration or precipitation of mixed dispersions of PANI and graphene. The highest specific capacitance of these composites was reached to 301 F/g. Murugan et al. [18] prepared PANI/graphene composites by in situ polymerization method using graphene directly reduced from GO. Cyclic voltammogram of this graphene/PANI nanocomposite showed a specific capacitance of 408 F/g. Wang et al. [13] synthesized graphene/polyaniline composite material by an in situ polymerization–reduction/dedoping–redoping process which showed an improved electrochemical behavior. A specific capacitance of 1,126 F/g was obtained for this graphene/polyaniline composite. Moreover, Zhang et al. [19] synthesized homogeneous graphene/polyaniline nanofiber composites by in situ polymerization of aniline in the presence of well-dispersed GO in acid solution followed by reduction in GO by hydrazine and re-oxidation and re-protonation of reduced polyaniline. They achieved a specific capacitance of 480 F/g for the prepared composite. Then, Du et al. fabricated PANI/GR hybrid via covalent grafting polymerization in the presence of GR and under acidic condition, to avoid free PANI particles and phase separation. However, the highest measured specific capacitance value for these hybrids was lower than that of the pure polyaniline (922 vs. 960 F/g) [20]. It can say that morphology changes that enhance the  $\pi$ – $\pi$

interaction of graphene sheets and PANI chains may assist the electron transfer and consequently improve the electrochemical properties of the prepared nanocomposites.

In this work, we introduced well-controlled graphene/emeraldine salt sandwich-like structure in order to increase surface area of PANI/graphene composites and subsequently coating of graphene sheets with conductive polymer to avoid free polyaniline particles which led to superior specific capacitance of the mentioned system. In this system, we synthesized a sheet-on-sheet structure with a high specific capacitance and no free particles of polyaniline. It is expected that the graphene/emeraldine salt nanocomposites with good sandwich-like structures would be promising in various applications. Since there is a need to accomplish graphene-based materials with improving electrical characteristic, good mechanical properties, excellent dispersibility in composites and worthy electrochemical properties, we encouraged to design a new method for preparation of the graphene/ES core–shell structure. The graphene used in this work has been prepared through the oxidation of graphite followed by reduction in the resulting graphene oxide. Subsequently, the graphene/emeraldine salt (GR/ES) sandwich-like structures were synthesized by the in situ inverse microemulsion polymerization of aniline in the presence of graphene. In this system, the graphene functions as an efficient dopant for the conducting polymer and plays a dual role as an electron acceptor and anionic counter ion. Morphology, characterization, electrical and electrochemical properties of the GR/ES sandwich-like structures were investigated, as well.

## Experimental

### Materials

Natural graphite was obtained from Ardabil Petrochemical Co., Iran. Aniline (analytical grade reagent) was purchased from Merck (Germany) and freshly distilled under reduced pressure before use. Ammonium persulfate (APS) (analytical grade reagent) was used as oxidant and received from Merck (Germany). Sodium dodecylbenzenesulfonate (SDBS), potassium permanganate ( $\text{KMnO}_4$ ) and hydrazine monohydrate were supplied from Sigma-Aldrich (USA). Sulfuric acid, hydrogen peroxide, *n*-hexane and butanol were of analytical grade and purchased from Merck (Germany). Doubly deionized water was used through all the processes.

### Synthesis of graphite oxide

The graphite oxide (GO) was first synthesized using Hummer's method [21] from the natural graphite powder with

the size of 120 meshes. Approximately 0.85 g of graphite flake was added to 23 mL of concentrated  $\text{H}_2\text{SO}_4$  by stirring, and then, it was cooled in an ice bath. Approximately 3 g of  $\text{KMnO}_4$  was added gradually by stirring, and the temperature of the mixture was maintained at 0 °C. The reaction continued for 8 h at 0 °C. In the next step, approximately 50 mL of distilled water was slowly added to the mixture and was maintained at the same temperature for 30 min. Finally, the reaction was terminated by the addition of 140 mL of 10 wt%  $\text{H}_2\text{O}_2$  solution. The product was filtered and washed repeatedly with 10 wt% HCl solution and then with acetone.

The prepared graphite oxide powder was dispersed in 200 mL distilled water using ultrasonic 150 % amplitude for 5 min. After centrifugation of the stable dispersion, the supernatant was filtered to avoid any unexfoliated graphite oxide. The yield of reaction was 70 %.

### Synthesis of graphene

Graphene (GR) was prepared from the graphene oxide by chemical reduction. In order to carry out the reduction, synthesized graphene oxide was dispersed in 250 mL of deionized water. Then, 10 mL of hydrazine monohydrate was added to the mixture and heated at 95 °C for 2 h. After the completion of the reaction, the graphene was collected by filtration as a black powder. The product thus obtained was washed with deionized water several times to remove excess hydrazine, and the final product was freeze-dried. The yield of reaction was 90 %.

### Synthesis of graphene/ES sandwich-like structures

#### *Preparation of inverse microemulsion system*

Typically, 6 g SDBS was added into 5 mL of 0.1 M HCl solution, and then, 3 mL butanol and 60 mL *n*-hexane were introduced. The mixture was stirred and turned into a transparent solution immediately. Thus, a stable, homogeneous and transparent inverse microemulsion system was acquired.

#### *Polymerization of aniline in microemulsion solution*

Various amounts of graphene (GR) were added into the samples of the obtained homogeneous inverse microemulsion solution and sonicated for 6 h until no trace of carbon remained and cooled to 0 °C.

On stirring, 0.33 mL (3.5 mmol) aniline monomer was dissolved in the resulting solution by stirring for 30 min. A solution of deionized water (5 mL) containing 1.2 g (5.3 mmol) ammonium persulfate was added slowly to the reaction mixture. After a few minutes, the dark suspension

changed to dark green color, implies the successful polymerization of aniline. The reaction was carried out at 0 °C under nitrogen while stirring for 24 h. The polymerization was finished by transferring the mixture into acetone, and then, the GR/ES composites precipitated. Finally, the mixture was filtered and washed with 0.1 M HCl solution and acetone to obtain the GR/ES sandwich-like structure. Then, the powder was freeze-dried before characterization.

The weight ratios of graphene in GR/ES samples were 1, 10 and 20 wt%, and the resulting nanocomposites were marked as GR/ES-1, GR/ES-10 and GR/ES-20, respectively.

### Characterization

Zeta potential of aqueous solution of graphene was measured by Zeta Sizer at 25 °C (Nano ZS, Malvern Instrument, UK). The surface morphologies of the graphene and GR/ES nanocomposites were observed using a scanning electron microscopy (SEM, S-4160, Hitachi, Tokyo, Japan). The sample was placed on an aluminum holder and then coated with a thin layer of gold. Further morphological investigation of materials was performed using a Zeiss LEO 906 transmission electron microscope (TEM, Oberkochen, Germany). The TEM samples were prepared by dispersing a small amount of powder sample in ethanol by ultrasonication. Then, a drop of suspension was placed on a carbon-coated grid. The grid was completely dried and used for TEM analysis (100 kV). The X-ray diffraction (XRD) patterns of the samples were recorded by a Bruker AXS D8 advanced diffractometer (Germany) using Cu ( $K\alpha$ ) radiation (wavelength: 1.5406 Å) at room temperature in  $2\theta$  ranges between 10° and 60° at a scanning rate of 2°/min.

Raman spectra were recorded with a Horiba Jobin-Yvon Raman microscope (Japan) at 514 nm with a charge-coupled device detector and graphite, graphene oxide as well as graphene powder were used for the test. Fourier transform infrared (FTIR) analysis was performed on a Bruker Equinox55 analyzer (Germany) equipped with a DTGS detector and a golden gate micro-ATR over a frequency range of 600–4,000  $\text{cm}^{-1}$ . The thermogravimetric analysis (TGA) was carried out on a thermal gravimetric analyzer (TGA Q50, TA instruments, USA) from ambient temperature to 800 °C under nitrogen flow at the heating rate of 20 °C/min. The thermal behavior was measured with a DSC Q100 from the TA instruments (USA) with the heating and cooling ramp of 10 °C  $\text{min}^{-1}$  from room temperature to 350 °C under argon flow. The amount of each samples was 2–2.5 mg.

Measurements of electrical conductivities of the pellet samples were performed using a Keithley 2000 (Keithley Instruments Inc., USA) apparatus. The resistivity of the

pressed samples was measured in a four-point probe unit using the following equations:

$$\begin{aligned} \text{Resistivity } (\rho, \text{ ohm.cm}) &= \pi t / \ln 2(V/I) \\ &= 4.53 \times t \times (\text{resistance}) \end{aligned} \quad (1)$$

$$\text{Conductivity } (\sigma, \text{ S/cm}) = 1/\rho \quad (2)$$

where,  $t$  is the thickness of the sample,  $V$  is the measured voltage and  $I$  is the source current.

Cyclic voltammograms of the different samples within a potential window from  $-0.2$  to  $1.0$  V were recorded on the Metrohm 757 VA Computrace (Herisau, Switzerland). The Pt as the counter electrode, an Ag/AgCl electrode as the reference electrode and a composite loaded glassy carbon as the working electrode were used in  $1$  M of  $\text{H}_2\text{SO}_4$  (aq.) at  $5$ ,  $10$ ,  $30$ ,  $50$  and  $100$  mV/s. For composite loading, each sample was dispersed in NMP with  $0.2$  mL of Nafion solution and sonicated in an ultrasonic bath for  $5$  min. Then, about  $40$   $\mu\text{L}$  of the mixture was coated on glassy carbon electrode and dried in air at  $60$   $^\circ\text{C}$  for  $5$  min.

X-ray photoelectron spectroscopy (XPS) graphs were acquired using a Gammatdata-Scientia ESCA 200 hemispherical analyzer equipped with an Al K $\alpha$  ( $1,486.6$  eV) X-ray source. All samples were mounted on standard sample holders by means of double-sided adhesive tapes.

## Results and discussion

### Synthesis and characterization of graphene

Graphene oxide was synthesized according to the modified Hummer method and then reduced to graphene by hydrazine hydrate. The measured zeta potential of graphene was  $-7.59$  mV, indicating the presence of negative charges on graphene surface. This negatively charged graphene may facilitate the growth of emeraldine salt.

Raman spectroscopy is a powerful tool to investigate the functionalization and the structural change in graphitic materials. The G band corresponding to the first-order scattering of the E $_{2g}$  mode arises primarily from in-plane  $\text{sp}^2$  carbon atoms, while the D band originates from  $\text{sp}^3$  carbon atoms that cause defects to emerge in the graphite. The D band is attributed to the reduced in-plane  $\text{sp}^2$  domain sizes in the pristine graphite, possibly due to extensive oxidation [22]. As shown in Fig. 1, GO has the D band at  $1,317.96$   $\text{cm}^{-1}$  and the G band at  $1,596.49$   $\text{cm}^{-1}$ , while graphene has the D and the G bands at  $1,314.56$  and  $1,588.11$   $\text{cm}^{-1}$ , respectively. The relative positions of the D and G bands are widened which indicates the aromatic restoration in the graphene structure. The intensity ratio of the D to the G bands ( $I_D/I_G$ ) can be used to indirectly assess the relative degree of functionalization or defects in the

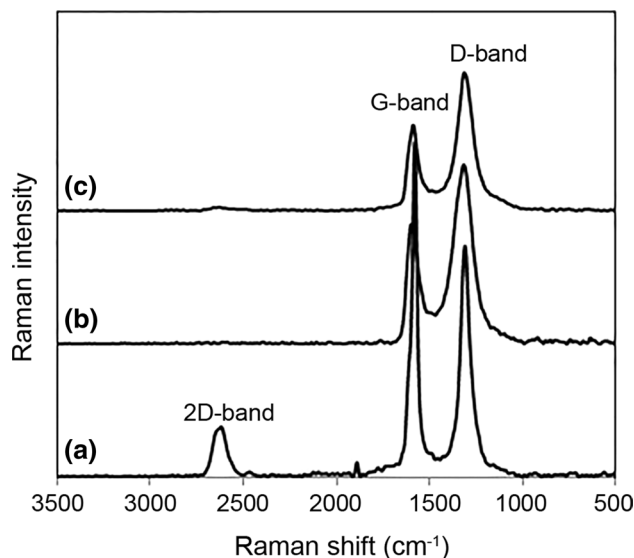


**Fig. 1** Raman spectra of graphite (a), graphene oxide (b) and graphene (c)

graphene. The  $I_D/I_G$  values are  $2.83$  and  $2.51$  for graphene and GO, respectively, which indicates that the average crystallite size of graphene was smaller than that of GO, when directly reduced by hydrazine hydrate. The enhanced ratio of the D/G intensities resulted from the formation of more numerous new graphitic domains, along with a decrease in the average size of the  $\text{sp}^2$  domains upon reduction of the graphene oxide [23].

Figure 2 shows FTIR spectra of graphite, graphene oxide and graphene. The characteristic vibrations of GO are clearly visible, such as for hydroxyl ( $3,390$   $\text{cm}^{-1}$ ), carboxylic acid ( $1,729$   $\text{cm}^{-1}$ ), C = O ( $1,618$   $\text{cm}^{-1}$ ) and C–O ( $1,054$ ,  $829$   $\text{cm}^{-1}$ ). In graphene spectrum, the carboxylic acid signal remained unchanged, while the other signals were reduced due to restoration of the most aromatic structure during chemical reduction, indicating that graphene still retained some defects or active sites which can help to the polymerization.

### Synthesis and characterization of GR/ES sandwich-like structures

In situ inverse microemulsion synthesis was the main technique for the synthesis of GR/ES nanocomposites. Scheme 1 shows the proposed mechanism for this synthesis. Initially, in the inverse microemulsion, the hydrophilic head groups of SDBS solvated in the water phase owing to their polarity; the hydrophobic groups extended into the oil phase and thus formed the SDBS inverted micelles. Some of SDBS micelles were adsorbed onto the outside surface of the well-dispersed graphene. The other micelles were dispersed in hexane, and a dynamic equilibrium was set

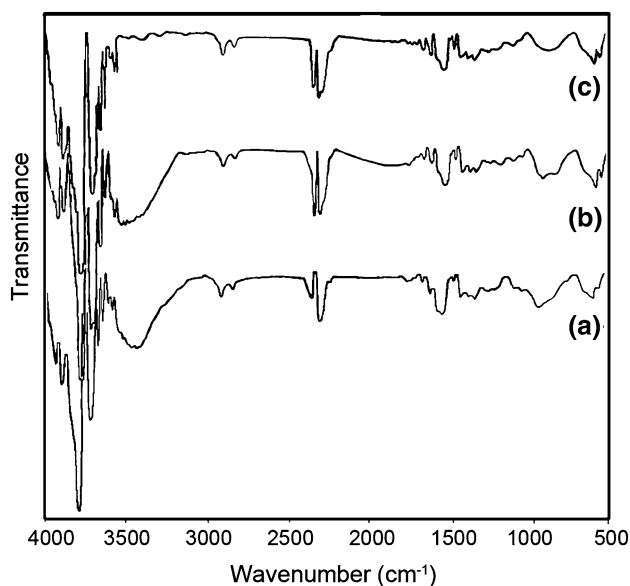


**Fig. 2** FTIR spectra of graphite (a), graphene oxide (b) and graphene (c)

up between the two phases. Once the aniline hydrochloride was added into the inverse microemulsion, they would reside in the SDBS micelles [24].

When initiator were added into the graphene dispersion, the aniline molecules adsorbed on the graphene sheets were started to polymerize just from the adsorbed sites on the surfaces [25]. When aniline hydrochloride encapsulated in adsorbed micelles had been oxidized, the residual aniline hydrochloride would be expected to diffuse toward the surface of the graphenes and be further oxidized until all the aniline dissolved in the solution was reacted. It is expected that  $\pi$ - $\pi$  stackings were formed between the polymer backbone and the graphene sheets [25]. The formation of the ES directly coated on the graphene nanosheets could arise from the strong interaction between the aniline monomer and graphene in the presence of SDBS. This interaction could be made up as a result of two reasons: (i) the

$\pi$ - $\pi$  electron interaction between the graphene and the aniline monomer and (ii) formation of the hydrogen bond between the carboxyl groups of the graphene and amine groups of the aniline monomers [25].

The resulting GR/ES nanostructures were stabilized by SDBS, as well. The product was precipitated in acetone to eliminate surfactants and initiators. The amount of ES coated on the surface of graphene is directly correlated to the initial concentration of aniline monomer in the solution. In particular, a higher concentration of aniline in the surrounding media of graphene led to the formation of more ES nuclei and a coarse shell.

#### Investigation of GR/ES sandwich-like morphology

Figure 3 shows the SEM micrographs of the graphite, graphene and GR/ES sandwich-like structures with different graphene ratios. Unlike the bulk synthesized ES (Fig. 3c, d), graphene (Fig. 3b) provided a smooth template for adhesion of as-synthesized ES in the case of sandwich-like GR/ES samples. The graphene coated with emeraldine salt (GR/ES-1) exhibited a coarse surface (Fig. 3e, f), whereas only the aniline monomers next to the graphene particles would be absorbed on the surface of graphene sheet. Consequently, the remained monomers in the surrounding medium endured homogeneous nucleation and growth in the solution. The SEM micrographs of the (GR/ES-1) and (GR/ES-10) samples showed that there were still emeraldine salt nanoparticles on the graphene sheets (Fig. 3e, g, respectively). However, when the sample with 20 wt% of graphene was coated with emeraldine salt, the surface of the GR/ES was smooth due to the absence of deposited emeraldine salt nanoparticles on the surface as shown in Fig. 3i, j.

It can be seen that the thickness of the GR/ES nanocomposites (Fig. 3e–j) increased in comparison with graphene (Fig. 3b) represented a successful coating of the graphene by emeraldine salt via oxidation polymerization. As shown in Fig. 3e, g and i, the layer structure that is a few

**Scheme 1** Proposed mechanism of formation of GR/ES sandwich-like structures

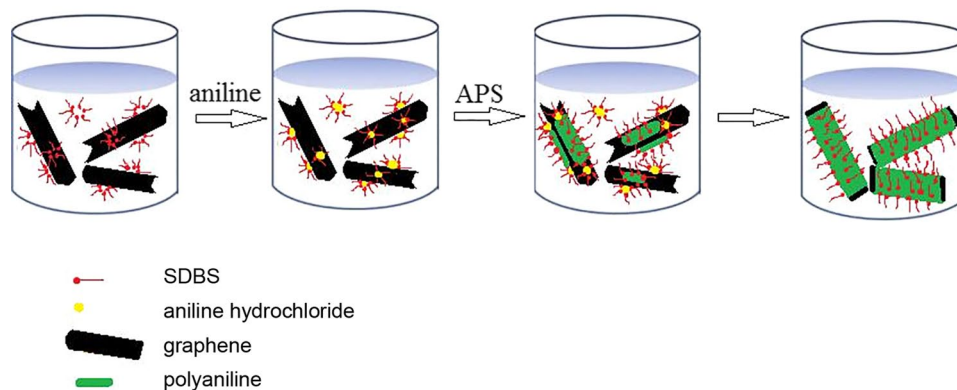
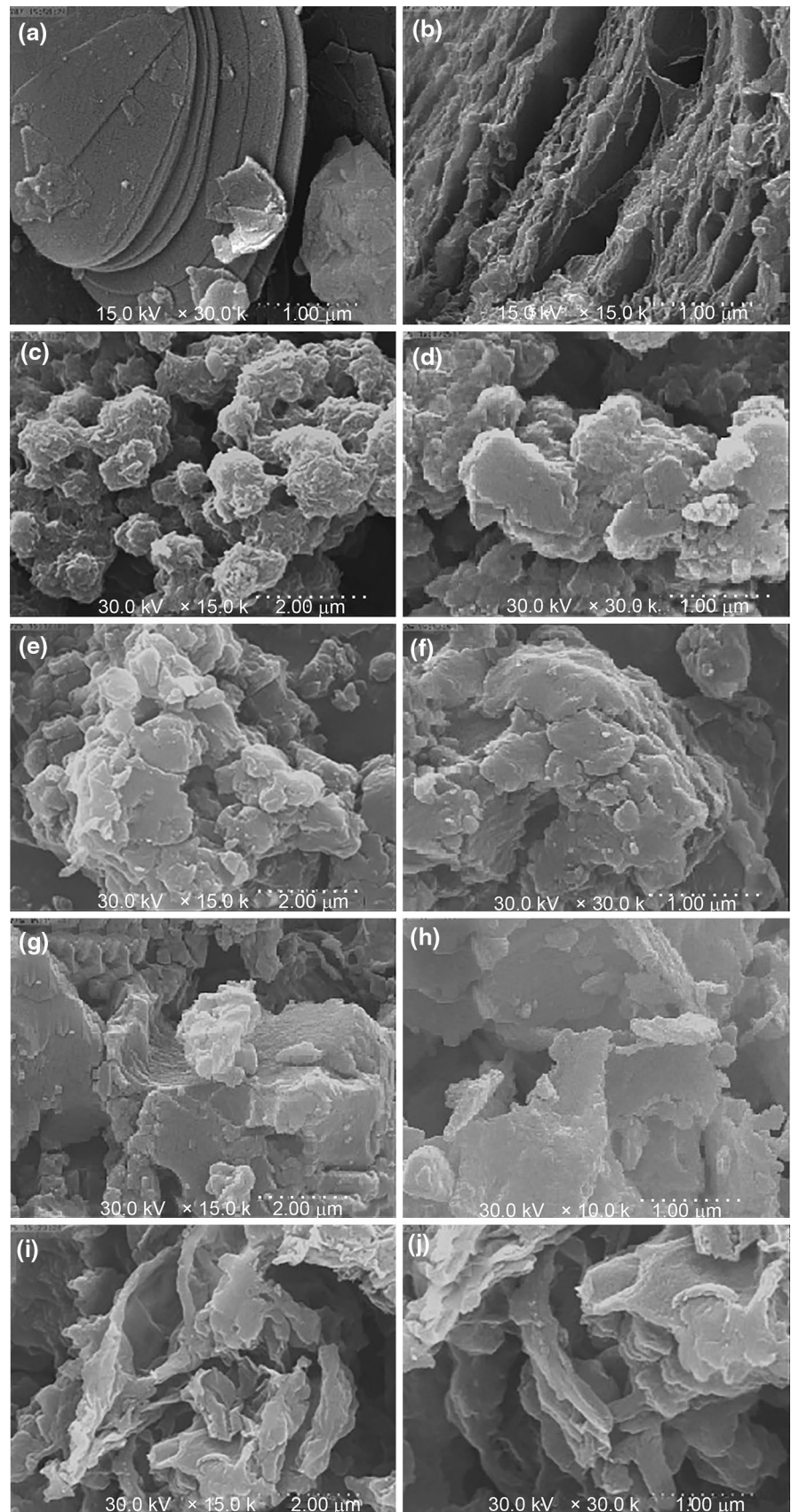


**Fig. 3** SEM micrographs of natural graphite (a), graphene (b), ES (c, d), GR/ES-1 (e, f), GR/ES-10 (g, h) and GR/ES-20 (i, j)



micrometers in length and approximately less than 50 nm in diameter indicated the graphene coated by polyaniline. In the GR/ES-20 sample (Fig. 3i), the emeraldine salt coatings were thinner compared to the emeraldine salt coatings in GR/ES-10 (Fig. 3g) and GR/ES-1 (Fig. 3e) samples. It is observed that the thin GR/ES layered structure can be obtained by increasing the graphene content.

It is well known that graphene is a good electron acceptor and aniline, on the other hand, is a very good electron donor [26]. When HCl is used as a dopant, therefore, the aniline monomer is expected to be absorbed onto the surface of graphene through electrostatic attraction and by the formation of weak charge-transfer complexes between aniline monomer and the graphitic structure of graphene. Hence, it is no doubt to say that the graphene can be considered as a falt template for emeraldine salt growth providing a large number of active nucleation sites. The thin ES coating on the surface of the graphene sheet as a template minimizes the distance between the dopant counter ion graphene and emeraldine salt chains rendering the ideal distance for an effective doping of emeraldine salt.

The morphology and structure of graphene, emeraldine salt and GR/ES-20 were further studied by TEM and SAED diffraction patterns (Fig. 4). It is obvious that GR/ES-20 is thicker in comparison with graphene, indicating ES coat on the surface of graphene and the graphene sheet retains its original layer-like structure.

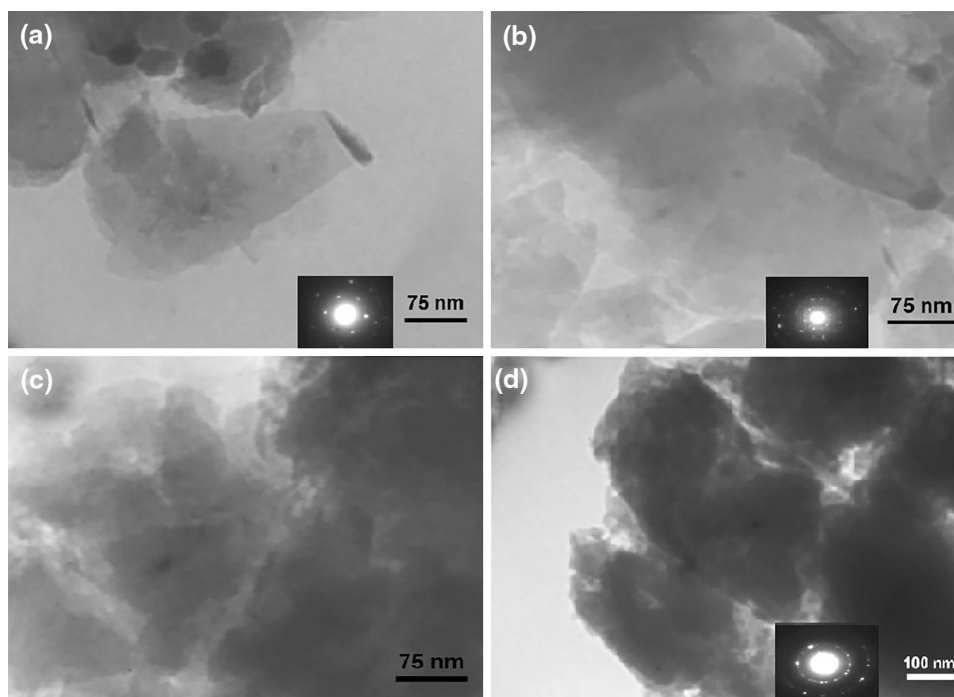
For further investigation, the selected area electron diffraction (SAED) patterns are shown as insets in Fig. 4. Spot pattern in the inset of Fig. 4a shows typical sixfold

rotational symmetry, which confirms the benzene-ring pattern of the graphene sheet [27]. The several sharp concentric rings observed in the pattern of ES suggest polycrystalline nature of this sample (Fig. 4b). Figure 4c, d shows particle-on-sheet and sheet-on sheet morphology for GR/ES-10 and GR/ES-20 samples, respectively. A comparison of the SAED patterns of GR/ES-20 and emeraldine salt discloses that with the addition of graphene to ES, the composite shows the new crystalline structures. This is due to charge-transfer processes, which happens at the contact interface between graphene and ES.

#### FTIR analysis

Figure 5 demonstrates FTIR spectra of graphene, emeraldine salt and their composites. The spectrum of emeraldine salt exhibits the bands at about 1,590 and 1,499  $\text{cm}^{-1}$  correspond to C–C stretching of quinoid and benzoid rings vibrations, respectively, indicating the oxidation state of emeraldine salt (ES). As commonly observed for emeraldine salts, the benzenoid band at 1,499  $\text{cm}^{-1}$  is more intense than that of the quinoid band at 1,590  $\text{cm}^{-1}$ . The strong characteristic band appearing at 1,146  $\text{cm}^{-1}$  was expressed by MacDiarmid and co-workers as the “electron-like band” and is considered to be a measure of the delocalization of the electrons which is indicative of the conductivity of emeraldine salt [28]. The peaks at 1,304 and 1,273  $\text{cm}^{-1}$  correspond to the C–N stretching vibrations. The peak at 804  $\text{cm}^{-1}$  is attributed to the out-of-plane bending of C–H. The weak shoulders at 2,980–3,050  $\text{cm}^{-1}$

**Fig. 4** TEM micrographs of graphene (a), ES (b), GR/ES-10 (c) and GR/ES-20 (d) (Insets show their corresponding electron diffraction patterns by SAED)



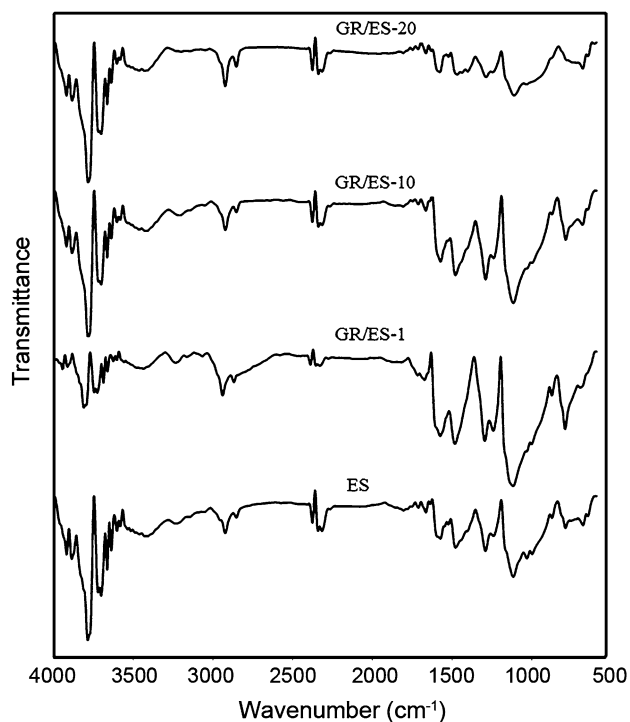


**Fig. 5** FTIR spectra of ES, GR/ES-1, GR/ES-10 and GR/ES-20 samples

correspond to aromatic  $sp^2$  CH stretchings. These bands suggest that emeraldine salt was formed in the emulsion during polymerization.

The FTIR spectra of the GR/ES nanocomposites match with that of the emeraldine salt. The peak appearing at  $1,711\text{ cm}^{-1}$  in spectrum of GR/ES samples arises from the graphene, which can be confidently assigned to the carbonyl stretching vibration. The ratio of intensity between quinoid and benzenoid rings has significant change for GR/ES nanocomposites at different graphene contents. The calculated ratio for the absorption intensity of quinoid to benzenoid ring modes ( $I_{1590}/I_{1499}$ ) in the emeraldine salt is 0.71, which suggests that the percentage of benzenoid units was much higher than that of the quinoid units. However, the ratio of  $I_{1590}$  to  $I_{1499}$  increased to 1.20, 1.97, 3.67 for GR/ES-1, GR/ES-10, GR/ES-20 samples, respectively, which indicated that the relative amount of quinoid units increased in the GR/ES samples polymerized in the presence of graphene. The  $\pi$ -bonded surface of graphene interacted with the conjugated structure of emeraldine salt, and as a result, the intensity ratio of quinoid to benzenoid increased. The benzenoid and quinoid peaks of emeraldine nanocomposites presented a red shift (Table 1), indicating that the  $\pi$ -bonded surface of graphene interacts with the conjugated structure of emeraldine salt.

Adsorption of the polymer onto the graphene surface and growth around the graphene will restrict vibrations

**Table 1** Changes in the vibration modes of GR/ES nanocomposites in comparison with ES

Vibration mode	ES	GR/ES-1	GR/ES-10	GR/ES-20
C = C benzenoid ring ( $\text{cm}^{-1}$ )	1,490	1,491	1,488	1,481
C = C quinoid ring ( $\text{cm}^{-1}$ )	1,590	1,587	1,582	1,581

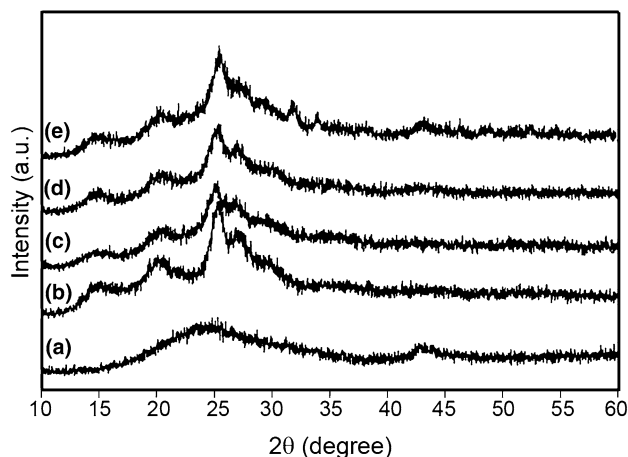


**Fig. 6** X-ray diffractograms of graphene (a), ES (b), GR/ES-1 (c), GR/ES-10 (d) and GR/ES-20 (e)

modes of polyaniline, which will lead to the differences in the FTIR spectra. This pronounced decrease suggests that an interaction between the quinoid ring of the doped emeraldine salt and the graphene may occur as a consequence of the in situ polymerization. This interaction then may facilitate charge-transfer processes between the components of the system and thus influence the transport properties. At first, addition of graphene to emeraldine salt resulted in the increment of H-bonding and consequently leading to reduction of the N–H stretching intensity (GR/ES-1). Then, after further addition of graphene, the interaction between the graphene and emeraldine salt may result in “charge transfer,” whereby the  $sp^2$  carbons of the graphene competed with dopant ions [ $\text{Cl}^-$ ] and perturbed the H-bond, resulted in an increase in the N–H stretching intensity (GR/ES-20).

#### XRD analysis

Figure 6 shows the X-ray diffraction patterns of the ES, graphene and GR/ES sandwich-like structure samples. There are three peaks at  $15.2^\circ$ ,  $20.4^\circ$  and  $25.4^\circ$  in the XRD pattern of the emeraldine salt [corresponding to (011), (020) and (200) amine salt crystals, respectively] [29] (Fig. 6, pattern b). The broad peak at  $2\theta = 15.2^\circ$  is assigned to the repeating unit of the emeraldine salt chain.



**Table 2** Data extracted from XRD patterns

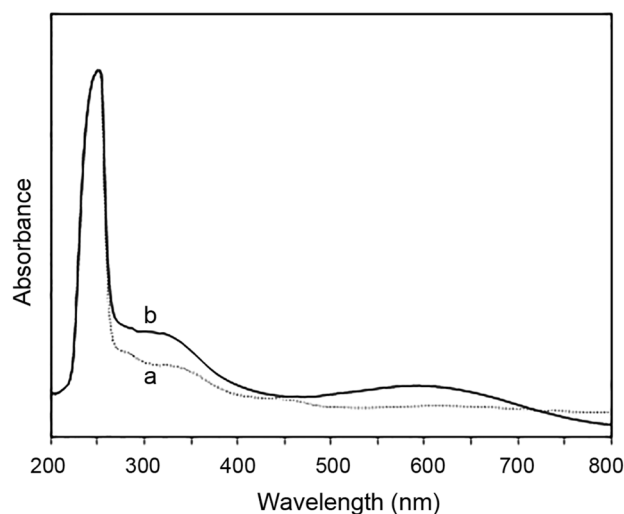
Sample code	$2\theta$	FWHM <sup>a</sup>	Crystallite size (nm)
ES	25.44	4.41	3.22
GR/ES-1	25.28	6.37	2.23
GR/ES-10	25.34	5.13	2.77
GR/ES-20	25.4	4.21	3.37

<sup>a</sup> Full width at half maximum of the diffraction

The peak centered at  $2\theta = 20.4^\circ$  is ascribed to periodicity perpendicular to the polymer chain. The peak at  $2\theta = 25.4^\circ$  is due to periodicity parallel to the polymer chain [assigned to (200) reflections] corresponding to the face-to-face interchain stacking between benzene rings [30]. It can be seen that the peak of  $2\theta = 25.4^\circ$  is stronger than that of  $2\theta = 20.4^\circ$ , due to highly doped emeraldine salt [31]. The graphene exhibits peaks at  $2\theta = 24.5^\circ$  and  $43.5^\circ$ , which correspond to the diffraction of the graphite (002) and (100), respectively. These peaks correspond to the few layer structures present in the sample [32]. The peak at  $2\theta = 24.5^\circ$  can be correlated to an interlayer spacing of 0.36 nm in the graphene sample.

The XRD pattern of the GR/ES displays the features of both the graphene and ES due to a hybrid of the graphene and emeraldine salt. For GR/ES nanocomposites, the peaks at  $2\theta = 15^\circ$  and  $20.4^\circ$  are similar to those of the pure emeraldine salt, indicating the unit structures of the emeraldine salt chain are unchanged after being loaded on the graphene, whereas the loading graphene changed the intensity of peak at  $2\theta = 25.4^\circ$ . A complete disappearance of graphene peak at  $2\theta = 24.5^\circ$  is obvious in GR/ES sandwich-like structure due to the insertion of emeraldine salt, which is embedded on the surface of graphene.

According to Table 2, by addition of graphene to emeraldine salt up to 1 wt%, the intensity of the peak at  $2\theta = 25.4^\circ$  decreased (GR/ES-1) at first, and then after further addition of graphene, the intensity of this peak enhanced by increasing graphene amount (i.e., GR/ES-10 and GR/ES-20). Crystallite size of emeraldine salt and GR/ES nanocomposites were calculated by Scherrer formula and listed in Table 2. As shown in Table 2, crystallite size of GR/ES-1 is reduced in comparison with emeraldine salt, but crystallite size of GR/ES-10 and GR/ES-20 increased in comparison with GR/ES-1 sample. The increase in peak intensity of nanocomposites with addition of graphene indicated an increase in the extension of microcrystalline domains in the sheet-on-sheet morphology in comparison with particle-on-sheet morphology, which is in agreement with the electrical conductivity of GR/ES-20. This is proposed that when less graphene was added, emeraldine salt crystals were disturbed; however, with further addition

**Fig. 7** UV spectra of ES (a) and GR/ES-1 (b)

of graphene, new crystals were formed around graphene sheets.

#### UV–Visible analysis

UV–Vis spectrum of emeraldine salt shows an intense absorption peak at 249 nm, a weak peak at 319 nm and a broad one at 450 nm (Fig. 7, spectrum a). The first and second absorption bands are related to the molecular conjugation ( $\pi$ – $\pi^*$  transition), while the third absorption peak is assigned to the polaron state of emeraldine salt, i.e., charged cationic species. The GR/ES-1 sample showed peaks located at 249, 334 and 590 nm (Fig. 7, spectrum b). Emeraldine salt bands at 319 and 450 nm were moved to higher wavelengths (red shift) in GR/ES-1 sample due to the interaction of polymer chain and graphene structure. The UV–Vis absorption results confirmed the strong interaction between the ES polymer and graphene sheets, which were in agreement with other analysis.

#### TGA analysis

Figure 8a shows the TGA thermogram of the graphene, ES and GR/ES samples. Graphene showed a low weight loss (approximately 15 %) up to 800 °C [33].

According to the DTG curves, the thermal degradation of the emeraldine salt and GR/ES showed a three-step weight loss process, as can be seen in Fig. 8b. In particular, the weight loss before 100 °C is due to some volatile species and the moisture adsorbed on emeraldine salt, while the weight loss within 200–300 °C could originate from the elimination of HCl as a dopant and bound water molecules acting as secondary dopant in emeraldine salt since synthesis was carried out in an aqueous medium.

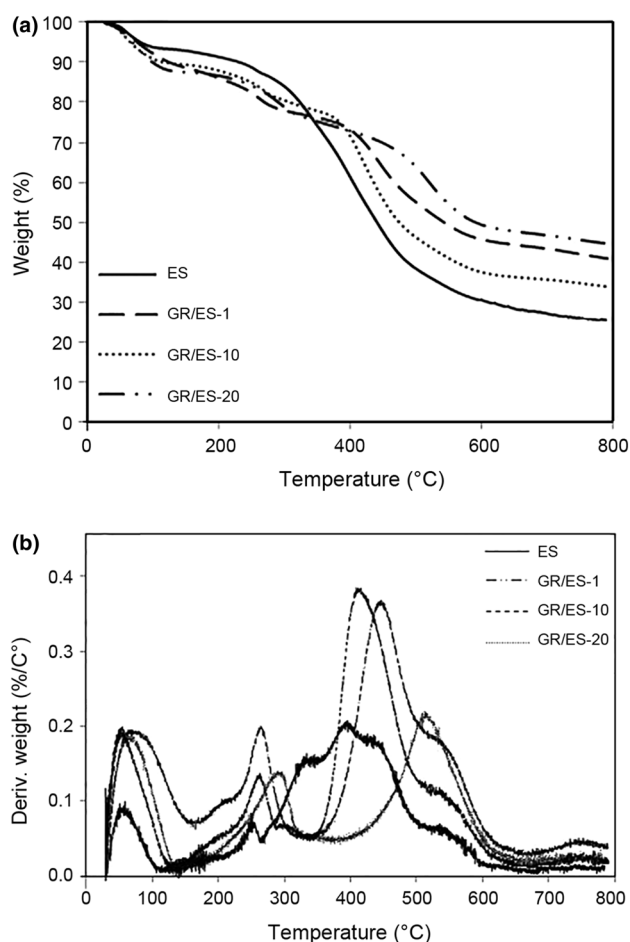


**Fig. 8** TGA thermograms of ES, GR/ES-1, GR/ES-10 and GR/ES-20 (a) and derivatives of weight loss vs. temperature for ES, GR/ES-1, GR/ES-10 and GR/ES-20 (b)

The major weight loss started from 300 °C corresponds to the thermal decomposition of the emeraldine salt [34] with a maximum thermal decomposition at approximately 394.50 °C for emeraldine salt. It was observed that the addition of graphene to the emeraldine salt could increase the thermal stability of related nanocomposites. For GR/ES-1 sample, maximum decomposition occurred at around 439.74 °C, which was 45 °C higher than the neat emeraldine salt, attributed to the high thermal properties of graphene composites. After 300 °C, mass loss of the GR/ES is relatively higher than that of the pure graphene based on the decomposition of the emeraldine salt component of the nanocomposites. These temperatures are listed in Table 3.

The increase in  $T_{\max 3}$  was due to the interaction between polymer (ES) chains and graphene which inhibited the degradation rate of polymer. These results provide additional evidence that ES interacted with the surface of the graphene sheets, leading to an enhanced thermal stability. This interfacial interaction reduced the mobility of the emeraldine salt around the graphene layers and led to an increase

**Table 3** Values of temperatures of weight losses obtained by DTG

Sample code	$T_{\max 1}$	$T_{\max 2}$	$T_{\max 3}$	$T_{50}^a$	Char yield (%) <sup>b</sup>
ES	56.81	251.60	394.50	435.58	24.81 %
GR/ES-1	66.27	257.74	439.74	467.33	31.13 %
GR/ES-10	67.83	263.43	410.36	469.34	33.79 %
GR/ES-20	69.11	292.82	514.62	588.34	44.77 %

<sup>a</sup> Temperature with a loss of 50 % of the initial mass

<sup>b</sup> Residual weight at 800 °C

in thermal stability. Thus, the PANI nanocomposites with graphene component showed better thermal stability with less mass loss compared with the polyaniline.

### DSC analysis

The study of the thermal behavior of GR/ES nanocomposites is of immense importance for interpreting the effect of graphene on emeraldine salt in these nanocomposites. The decomposition temperature of emeraldine salt before and after mixing with different amounts of graphene were investigated through DSC (Fig. 9).

Two endothermic peaks in DSC thermogram of pure ES and ES nanocomposites were observed; these peaks were most likely due to the evaporation of water ( $T_1$ ), evaporation of dopant ( $T_2$ ), respectively. These temperatures are listed in Table 4.

Emeraldine salt is known to be a hygroscopic polymer. Some authors assigned the endothermic effect registered by DSC in the range from ambient temperature up to approximately 120 °C to the evaporation of water [35]. With further addition of graphene to GR/ES samples, the ratio of emeraldine salt in nanocomposites was decreased and the temperature of evaporation of water decreased, as well. The restricted mobility of the polymer chains around the graphene sheets and the interfacial  $\pi$ - $\pi$  bond interactions between them in GR/ES nanocomposites also explain the increase in the  $T_2$  decomposition temperature and their thermostability in comparison with emeraldine salt.

### DC electrical conductivity

The DC electrical conductivities of graphene/ES were determined on pressed pellets from powder using a four-probe resistivity measurement system, and the average conductivities were collected. The electrical conductivities of emeraldine salt and (GR/ES) samples are shown in Fig. 10. For GR/ES-20 sample, the value of electrical conductivity was found to be as high as 5.4 S/cm, which was stable and reproducible over a period of time, indicating that the conductive networks in the system were well established. This discrepancy may arise due to the increased  $\pi$ - $\pi$

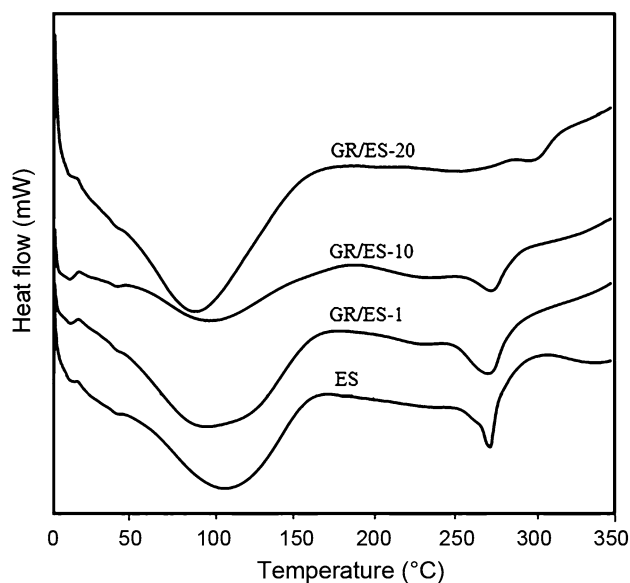


**Fig. 9** DSC thermograms of ES and GR/ES nanocomposites

**Table 4** Obtained decomposition temperatures of ES and GR/ESs by DSC

Sample code	$T_1$	$T_2$
ES	106.65	272.3
GR/ES-1	95.91	270.94
GR/ES-10	97.07	272.72
GR/ES-20	88.27	296.97

**Table 5** Specific capacitances of various samples at different scan rates

Sample	5 (mV/s)	10 (mV/s)	30 (mV/s)	50 (mV/s)	100 (mV/s)
Graphene	137.17	104.96	86.76	63.06	41.37
ES	129.88	125.63	88.27	71.08	54.77
GR/ES-1	262.58	297.37	200.79	157.81	106.44
GR/ES-10	71.72	61.54	41.63	34.19	25.24
GR/ES-20	1,615.42	1,504.48	1,312.72	1,176.60	982.35

interactions between emeraldine salt and graphene in the nanocomposite with sheet-on-sheet morphology in comparison with particle-on-sheet morphology.

In these sandwich-like structures, both components (polyaniline in emeraldine salt state and graphene) are electrically conducting materials. The graphene can bridge to transport the carrier by means of the  $\pi$ - $\pi$  interactions with emeraldine salt, which can improve the carrier mobility and thus increase the electrical conductivity of GR/ES nanocomposites. In comparison with ES, conductivity was decreased for

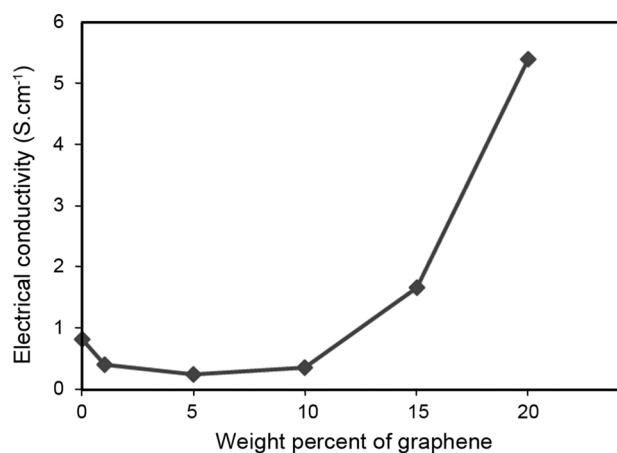


**Fig. 10** Four-point conductivity values for pressed pellets of ES and GR/ES nanocomposites

the samples with low amount (i.e., small fraction) of graphene and then increased with further addition of graphene.

At first, addition of graphene prevented the growth of crystallization and formed barriers to carrier transport in the emeraldine salt chains, which was consistent with the XRD results in Fig. 6. It is shown that the crystallite size of emeraldine salt was affected by the variation in the content of graphene in the resulting nanocomposites, and the changes in measured electrical conductivity should be then corresponded to changes in morphology of nanocomposites and crystallite size of emeraldine salt. Long et al. [36] have reported that bulk conductivity of nanostructured conducting emeraldine salt was based on the contact resistance between particles and generally was not representative of the real conductivity of the emeraldine salt. They estimated that inter-tubular contact resistance between two-crossed polyaniline/nanotubes can reach 500 k $\Omega$ , i.e., about 16 times superior than the intra-tube resistance of an individual PANI nanotube. Hence, it was found straightforwardly that the measured conductivity of the material was strongly influenced by crystallite size. Therefore, electrical conductivity of emeraldine salts with low amount of graphene (up to 10 wt%) descended and ascended with the addition of graphene (i.e., GR/ES-15 and GR/ES-20 samples).

The PANI/graphene composites prepared by the in situ polymerization have a graphene-like layered structure with PANI nanofibers intercalated between the layers and have showed conductivity of 231.2 S/m [19]. The maximum conductivity of chemically modified polyaniline nanocomposites by poly (2-acrylamido-2-methyl-1-propanesulfonic acid)/graphene nanoplatelet which was prepared via in situ deposition was 0.86 S cm<sup>-1</sup> [37].

The conductivity of the sulfonated polyaniline/graphene composite film prepared by filtration method was measured to be 0.3 S cm<sup>-1</sup>. The content of SPANI in this film was

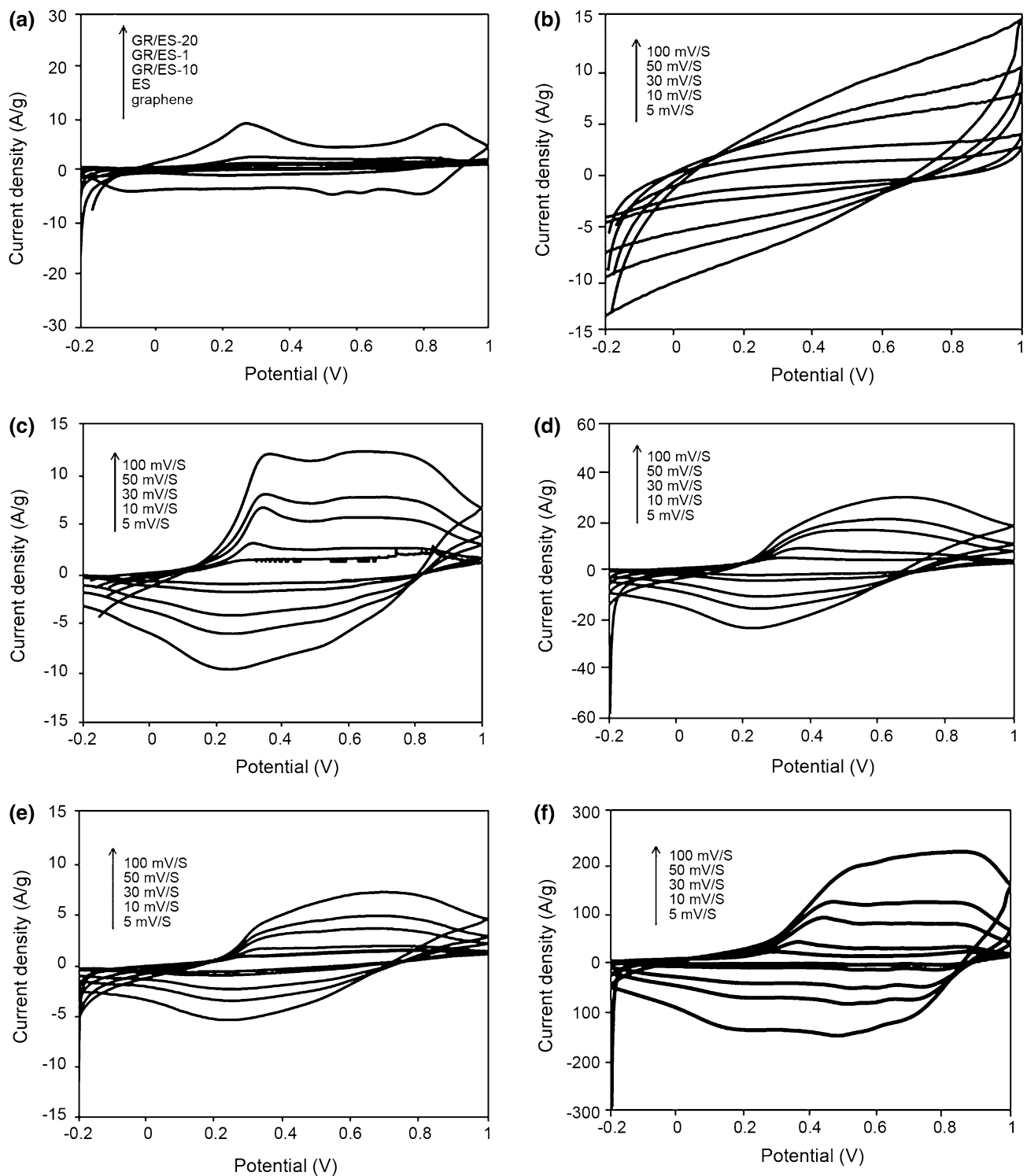


**Fig. 11** Cyclic voltammograms of graphene, ES, GR/ES-1, GR/ES-10, GR/ES-20 electrodes at a scan rate of 5 mV/s in 1 M  $\text{H}_2\text{SO}_4$  (a) and of graphene (b), ES (c), GR/ES-1 (d), GR/ES-10 (e) and GR/ES-20 (f) electrodes at different scan rates of 5, 10, 30, 50 and 100 mV/s

low, because a large amount of SPANI was passed through the filtration membrane during filtration [38]. The conductivity of SPANI/graphene composite film prepared by drop casting was  $0.03 \text{ S cm}^{-1}$  [38].

This improved electrical conductivity property in GR/ES-20 can be ascribed to the charge-transfer effect of the graphene and emeraldine salt in nanocomposites with sheet-on-sheet morphology.

## Electrochemical analysis

The electrochemical performances of the graphene/emeraldine salt nanocomposites were studied, and the results are shown in Fig. 11. The CV curves of ES, graphene, GR/ES-1, GR/ES-10 and GR/ES-20 samples which are shown in Fig. 11a were obtained at the scan rate of 5 mV/s in 1 M sulfuric acid aqueous solution in the potential range from  $-0.2$  to  $1.0$  V.

The graphene electrode exhibited an approximated rectangular shape which is characteristic of an electric double-layer capacitance (EDLC) behavior [39]. The PANI electrode showed a pair of redox peak that is characteristic of a pseudo-capacitance. Two couples of the redox peaks were observed from the CV curve of the ES attributed to the redox of polyaniline, corresponding to its leucoemeraldine/emeraldine and emeraldine/permanganiline structural transformations, respectively [40]. On the other hand, the CV curves of GR/ES samples show a behavior characteristic of a combination of both EDLC and redox capacitance.

The peak currents and CV loop area of the GR/ES nanocomposites were both much larger than that of ES and graphene. This may be contributed to the enhanced electron transfer efficiency of the sandwich-like structures which indicates the electrochemical performances of GR/ES nanocomposites. The electrochemical performances of the nanocomposites were enhanced compared with graphene and ES, due to the synergistic effect between graphene and ES. Among various samples, GR/ES-20 sample with sheet-on-sheet morphology had the largest area surrounded by the CV curve, indicating a higher specific capacitance indicating the electrochemical properties of this sample was advancing. Graphene, ES, GR/ES-1, GR/ES-10 and GR/ES-20 samples as the electrode were tested at various scan rates, and their voltagrams are shown in Fig. 11b–f.

With increasing scan rate, the redox current increased clearly, indicating the good rate capability for this electrode. Due to the resistance of the electrode, in the case of sandwich-like structure, the oxidation peaks shifted positively and the reduction peaks shifted negatively [14] with the increasing of sweep rates from 5 to 100 mV/s. However, the shifting was less than 0.2 V because of the enhanced charge transfer between the emeraldine salt and graphene.

To quantitatively evaluate the charge storage capacity from CV curve, the specific capacitance of the samples was determined by the expression voltammetric charge/(potential window  $\times$  composite loading) [41]. The specific capacitance was calculated accurately on the basis of the following equation:

$$C = \int_{E_1}^{E_2} i(E)d(E)/2(E_2 - E_1)v. \quad (3)$$

The GR/ES-20 electrode displayed a specific capacitance of 1,615.42 F/g at a scan rate of 5 mV/s, which was much higher than that of ES (129.88 F/g) and that of graphene (137.17 F/g) at the same scan rates. It is implied that the layered structures with sheet-on-sheet morphology shorten the diffusion lengths of the electrolyte ions and provide high electroactive regions (Table 5).

The specific capacitance was gradually decreased with increasing scan rate, because the diffusion occurred typically on the surface of the material placed on the electrode, not inside the bulk. With increasing scan rate up to

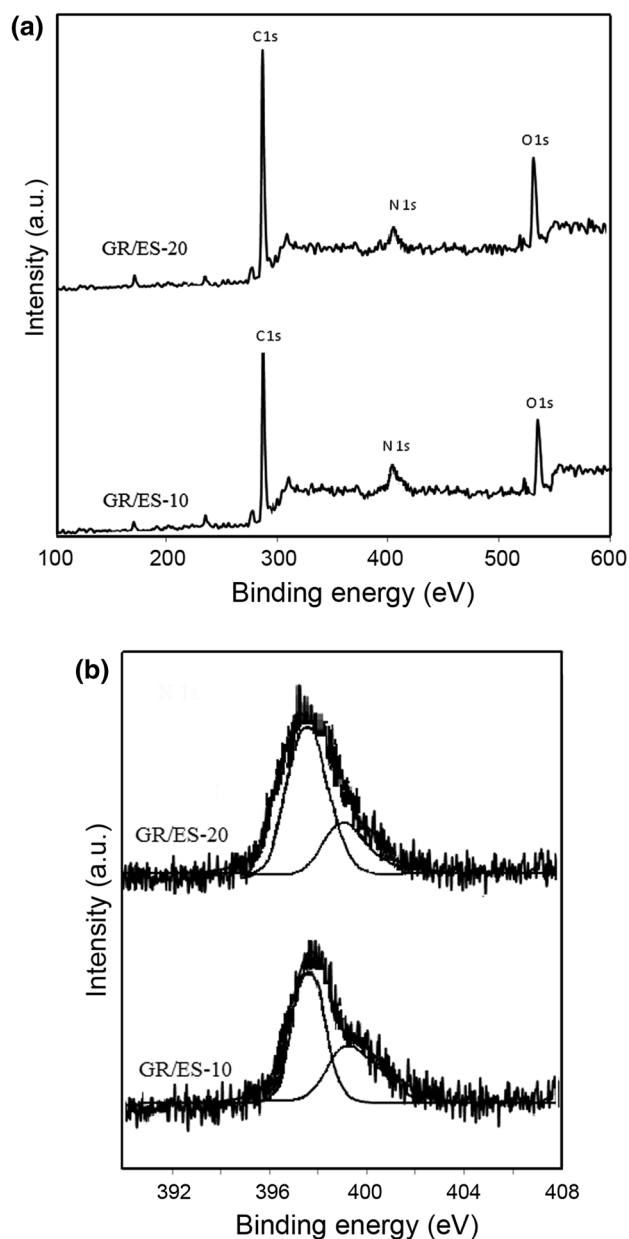


**Fig. 12** XPS spectra of GR/ES-10 and GR/ES-20 (a) and N1s core-level XPS spectra of GR/ES-10 and GR/ES-20 samples (b)

100 mV/s, GR/ES-20 sample still exhibited specific high capacitance of 982.35 F/g due to strong absorption of the components to each other and performing of an appropriate charge-transfer interaction. The specific capacitance of the GR/ES-20 electrode (1,615 F/g) at a scan rate of 5 mV/s is one of the best reports for capacitance based on carbon material and polyaniline [42–44].

Lower conductivity of GR/ES-10 with particle-on-sheet morphology resulted in the lower specific capacitance, which is in agreement with conductivity results. These preliminary results encouraged us to explore possible applications of GR/ES sandwich-like structures in various electrochemical devices in our future works.

### XPS analysis

Figure 12a shows the XPS spectra of GR/ES-10 and GR/ES-20 samples, where the corresponding N1s, C1s and O1s signals were presented. The graphitic carbon (C = C) was evident in the C1s spectrum at 284.6 eV. The presence of N1s core-level peak confirms the presence of emeraldine salt in the samples. The deconvolution of the N1s XPS spectra for GR/ES-10 and GR/ES-20 composites is depicted in Fig. 12b. Curve fitting of the N1s core-level spectrum of the GR-PANI composite in Fig. 12b assigned two distinctive peaks which were due to the presence of quinoid amine and benzenoid amine discovered at a binding energy of 397.8 and 399.2 eV. The corresponding ratio of quinoid amine to benzenoid amine was calculated from the integral area which were 1.83 and 3.35 for GR/ES-10 and GR/ES-20 samples, respectively. Therefore, the doping level of the emeraldine salt in sheet-on-sheet morphology was increased, which was consistent with the results of FTIR. The changes in the benzoid/quinoid ratio may have been due to the  $\pi$ - $\pi$  interactions between graphene and emeraldine salt chains, which may cause a synergistic effect on electrochemical properties of the composite.

### Conclusion

In summary, we have synthesized the graphene/emeraldine salt (GR/ES) sandwich-like structures using in situ inverse microemulsion polymerization. It was confirmed that the strongly conjugated interactions in the composites with uniform layered structures should greatly facilitate the charge-transfer interactions between the two components, thus showed enhanced electrical properties and thermal stability. The effect of the graphene ratio on the electrical properties of the GR/ES nanocomposites was also investigated. It was found that the sample with a graphene content of 20 wt% was uniformly coated with emeraldine salt leading to nanocomposite with separated layers structure and

fantastic electrical conductivity. Among the various investigated GR/ES sandwich-like structures, the GR/ES-20 sample exhibited a specific capacitance of 1615.42 F/g at a scan rate of 5 mV/s which recommended a new material for fabricating electrochemical devices.

**Acknowledgments** We are thankful to the Research Council of the University of Tehran. The authors gratefully acknowledged the kind assistance of Ms. A. Fotouhi at Polymer and Thermal Analysis Laboratory of the University College of Science, University of Tehran for TGA and DSC analyses.

### References

1. Cao J, Sun JZ, Hong H, Li HY, Chen HZ, Wang M (2004) Carbon nanotube/CdS core-shell nanowires prepared by a simple room-temperature chemical reduction method. *Adv Mater* 16:84–87
2. Huang X, Yin Z, Wu S, Qi X, He Q, Zhang Q, Yan Q, Boey F, Zhang H (2011) Graphene-based materials: synthesis, characterization, properties, and applications. *Small* 7:1876–1902
3. Zhou X, Wu T, Hu B, Yang G, Han B (2010) Synthesis of graphene/polyaniline composite nanosheets mediated by polymerized ionic liquid. *Chem Commun* 46:3663–3665
4. Huang YF, Lin CW (2012) Polyaniline-intercalated graphene oxide sheet and its transition to a nanotube through a self-curling process. *Polymer* 53:1079–1085
5. Pei QX, Sha ZD, Zhang YW (2011) A theoretical analysis of the thermal conductivity of hydrogenated graphene. *Carbon* 49:4752–4759
6. Wu Q, Xu Y, Yao Z, Liu A, Shi G (2010) Supercapacitors based on flexible graphene/polyaniline nanofiber composite films. *ACS Nano* 4:1963–1970
7. Bunch JS, Van der Zande AM, Verbridge SS, Frank IW, Tanenbaum DM, Parpia JM, Craighead H, McEuen PL (2007) Electromechanical resonators from graphene sheets. *Science* 315:490–493
8. Stankovich S, Dikin DA, Dommett G, Kohlhaas K, Zimney E, Stach E, Piner R, Nguyen S, Ruoff R (2006) Graphene-based composite materials. *Nature* 442:282–285
9. Yao J, Shen X, Wang B, Liu H, Wang G (2009) In situ chemical synthesis of SnO<sub>2</sub>-graphene nanocomposite as anode materials for lithium-ion batteries. *Electrochem Commun* 11:1849–1852
10. Ashraf R, Kausar A, Siddiq M (2014) High-performance polymer/nanodiamond composites: synthesis and properties. *Iran Polym J* 23:531–545
11. Deng L, Wang J, Liang J, Zhu G, Kang L, Hao Z, Lei Z, Yang Z, Liu Z (2014) RuO<sub>2</sub>/graphene hybrid material for high performance electrochemical capacitor. *J Power Sources* 248:407–415
12. Xu Y, Wang Y, Liang J, Huang Y, Ma Y, Wan X, Chen Y (2009) A hybrid material of graphene and poly (3,4-ethyldioxythiophene) (PEDOT) optical transparency with high conductivity, flexibility, and transparency. *Nano Res* 2:343–348
13. Wang HL, Hao QL, Yang XJ, Lu LD, Wang X (2010) A nanostructured graphene/polyaniline hybrid material for supercapacitors. *Nanoscale* 2:2164–2170
14. Ramanathan T, Abdala AA, Stankovich S, Dikin DA, Herrera-Alonso M, Piner RD, Adamson DH, Schniepp HC, Chen X, Ruoff RS, Nguyen ST, Aksay IA, Prud'Homme RK, Brinson LC (2008) Functionalized graphene sheets for polymer nanocomposites. *Nat Nanotechnol* 3:327–331
15. Wang YG, Li HQ, Xia YY (2006) Ordered whisker like polyaniline grown on the surface of mesoporous carbon and its electrochemical capacitance performance. *Adv Mater* 18:2619–2623

16. Luo YC, Do JS (2004) Urea biosensor based on PANi(urease)-Nafion/Au composite electrode. *Biosens Bioelectron* 20:15–23
17. Liu S, Liu X, Li Z, Yang S, Wang J (2011) Fabrication of free-standing graphene/polyaniline nanofibers composite paper via electrostatic adsorption for electrochemical supercapacitors. *New J Chem* 35:369–374
18. Murugan AV, Muraligant T, Manthiram A (2009) Rapid, facile microwave-solvothermal synthesis of graphene nanosheets and their polyaniline nanocomposites for energy storage. *Chem Mater* 21:5004–5006
19. Zhang K, Zhang LL, Zhao XS, Wu J (2010) Graphene/polyaniline nanofibers composites as supercapacitor electrodes. *Chem Mater* 22:1392–1401
20. Du F, Wang J, Tang C (2013) Enhanced electrochemical capacitance of polyaniline/graphene hybrid nanosheets with graphene as templates. *Compos B* 53:376–381
21. Hummers WS, Offeman RE (1958) Preparation of graphitic oxide. *J Am Chem Soc* 80:1339
22. Tuinstra F, Koenig JL (1970) Raman spectrum of graphite. *J Chem Phys* 53:126–1130
23. Sarker AK, Hong JD (2012) Layer-by-layer self-assembled multilayer films composed of graphene/polyaniline bilayers: high-energy electrode materials for supercapacitors. *Langmuir* 28:12637–12646
24. Lin Y, Rao AM, Sadanadan B, Kenik EA, Sun YP (2002) Functionalizing multiple walled carbon nanotubes with aminopolymers. *J Phys Chem B* 106:1294–1298
25. Feng W, Bai XD, Lian YQ, Liang J, Wang XG, Yoshino K (2003) Well-aligned polyaniline/carbon nanotube composite films grown by in situ aniline polymerization. *Carbon* 41:1551–1557
26. Singh K, Ohlan A, Pham VH, Balasubramanian R, Varshney S, Jang J, Hur SH, Choi WM, Kumar M, Dhawan SK, Kongd B, Chung JS (2013) Nanostructured graphene/Fe<sub>3</sub>O<sub>4</sub> incorporated polyaniline as a high performance shield against electromagnetic pollution. *Nanoscale* 5:2411–2420
27. Stankovich S, Dikin D, Dommett G, Kohlhaas K, Zimney E, Stach E (2006) Graphene-based composite materials. *Nature* 442:282–286
28. QuilSmrd S, Louarn G, Lefrant S, MacDiarmid AG (1994) Vibrational analysis of polyaniline: a comparative study of leucoemeraldine, emeraldine, and permigraniline bases. *Phys Rev B* 50:12496–12508
29. Ginic-Markovic MG, Matison J, Cervini R, Simon GP, Fredericks PM (2006) Synthesis of new polyaniline/nanotube composites using ultrasonically initiated emulsion polymerization. *Chem Mater* 18:6258–6265
30. Reddy K, Sin B, Ryu K, Noh J, Lee Y (2009) In situ self-organization of carbon black–polyaniline composites from nanospheres to nanorods: synthesis, morphology, structure and electrical conductivity. *Synth Met* 159:1934–1939
31. Singla ML, Sajeela A, Srivastava A, Jain DVS (2007) Effect of doping of organic and inorganic acids on polyaniline/Mn<sub>3</sub>O<sub>4</sub> composite for NTC and conductivity behaviour. *Sens Actuators A* 136:604–612
32. Raidongia K, Nag A, Hembram KPSS, Waghmare UV, Datta R, Rao CNR (2010) BCN: a graphene analogue with remarkable adsorptive properties. *Chem Eur J* 16:149–157
33. Moon I, Lee J, Ruoff RS, Lee H (2010) Reduced graphene oxide by chemical graphitization. *Nat Commun*. doi:10.1038/ncomms1067
34. Lee D, Char K (2002) Thermal degradation behavior of multi-walled carbon nanotubes/polyamide 6 composites. *Polym Degrad Stabil* 75:555–560
35. Yue J, Epstein AJ, Zhong Z, Gallagher PK, MacDiarmid AG (1991) Thermal stabilities of polyaniline. *Synth Met* 41:765–768
36. Long YZ, Yin ZH, Chen ZJ (2008) Low-temperature magnetoresistance studies on composite films of conducting polymer and multiwalled carbon nanotubes. *J Phys Chem C* 112:11507–11512
37. Basavaraja C, Noh GT, Huh DS (2013) Chemically modified polyaniline nanocomposites by poly(2-acrylamido-2-methyl-1-propanesulfonicacid)/graphene nanoplatelet. *Colloid Polym Sci* 291:2755–2763
38. Bai H, Xu Y, Zhao L, Li C, Shi G (2009) Non-covalent functionalization of graphene sheets by sulfonated Polyaniline. *Chem Commun* 13:1667–1669
39. Wei L, Tang DM, He YB, You CH, Shi ZQ, Chen XC, Chen CM, Hou PX, Liu C, Yang QH (2009) Low-temperature exfoliated graphenes: vacuum-promoted exfoliation and electrochemical energy storage. *ACS Nano* 3:3730–3736
40. Zhang LL, Li S, Zhang JT, Guo P, Zheng J, Zhao XS (2010) Enhancement of electrochemical performance of macroporous carbon by surface coating of polyaniline. *Chem Mater* 22:1195–1202
41. Conway BE (1999) *Electrochemical supercapacitors: scientific fundamentals and technological applications*. Kluwer, New York
42. Yan J, Wei T, Shao B, Fan ZJ, Qian WZ, Zhang ML, Wei F (2010) Preparation of a graphene nanosheet/polyaniline composite with high specific capacitance. *Carbon* 48:487–493
43. Yu P, Li Y, Zhao X, Wu L, Zhang Q (2014) Graphene-wrapped polyaniline nanowire arrays on nitrogen-doped carbon fabric as novel flexible hybrid electrode materials for high-performance supercapacitor. *Langmuir* 30:5306–5313
44. Feng XM, Li RM, Ma YW, Chen RF, Shi NE, Fan QL, Huang W (2011) One step electrochemical synthesis of graphene/polyaniline composite film and its applications. *Adv Funct Mat* 21:2989–2996